THE JOURNAL OF PHYSICAL CHEMISTRY B

ARTICLE

pubs.acs.org/JPCB

Surfactant Self-Assembly Nanostructures in Protic Ionic Liquids

B. Fernández-Castro,[†] T. Méndez-Morales,[†] J. Carrete,[†] E. Fazer,[§] O. Cabeza,[‡] J. R. Rodríguez,[†] M. Turmine,[§] and L. M. Varela*[,†]

[†]Grupo de Nanomateriales y Materia Blanda, Departamento de Física de la Materia Condensada, Universidade de Santiago de Compostela, Campus Vida s/n E-15782, Santiago de Compostela, Spain

[‡]Facultad de Ciencias, Universidade de A Coruña, Campus A Zapateira s/n E-15008, A Coruña, Spain

[§]Laboratoire Interfaces et Systèmes Electrochimiques, Université Pierre et Marie Curie-PARIS6, CNRS, UPR15-LISE, Paris, F-75005 France

ABSTRACT: The existence and properties of mesoscopic self-assembly structures formed by surfactants in protic ionic liquid solutions are reported. Micellar aggregates of *n*-alkyltrimethylammonium (n = 10, 12, 14, 16) chlorides and bromides and of *n*-alkylpyridinium (n = 12, 16) chlorides in ethylammonium nitrate and propylammonium nitrate were observed by means of several experimental techniques, including surface tension, transmission electron micrography, dynamic light scattering, and potentiometry using surfactant-selective electrodes. The effect of the alkyl chain length of both solute and solvent molecules on the critical micelle concentration is discussed, and a Stauff−Klevens law is seen to apply to surfactant solutions in both protic ionic liquids. The counterion role is also a matter of study in the case of alkyltrimethylammonium-based surfactants, and the presently reported evidence suggests that the place of the surfactant counterion in the Hoffmeister's series could determine its effect on micellization in IL solution. The size distribution of the aggregates is also analyzed together with the Gibbs free energies of micellization and the minimum surface area per monomer in all of the studied cases. All of the hereby reported evidence suggests that the negative entropic contribution arising from the release of the solvent layer upon micellization is also the driving force of conventional surfactant self-association in protic ionic liquids.

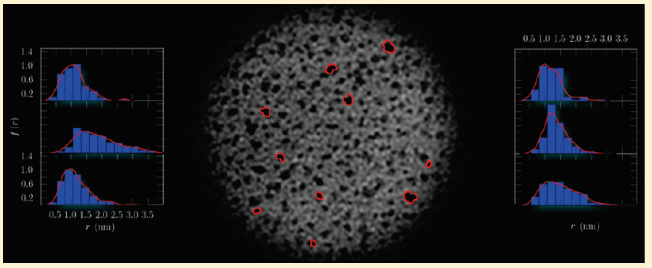

1. INTRODUCTION

Ionic liquids (ILs) or room-temperature molten salts are presently reputed to be novel materials of extreme importance in many academic and industrial applications. They exhibit some well-known tunable properties that confer them a central role as "designer solvents" in the so-called "green" branch of contemporary chemistry; these include negligible vapor pressure, nonflammability, ability to dissolve an enormous range of inorganic, organic, and polymeric materials at very high concentrations, noncorrosiveness, low viscosity, and so forth. In the early 1990s, Wilkes et al.[1] synthesized air- and water-stable IL C_2MIMBF_4 (1-ethyl-3-methylimidazolium tetrafluoroborate). This allowed a much wider range of applications than its homologous systems known since the final decades of the 19th century (ethylammonium nitrate, EAN, alkylimidazolium and alkylpyridinium mixtures of ILs, etc.). Since then, the number of reported contributions per year has grown exponentially, and ILs are now among the most active research fields in chemical physics.

On the other hand, it has been a very well known fact for decades that amphiphilic molecules with water-loving polar (hydrophilic) and water-hating nonpolar (hydrophobic) parts in their molecular structure tend to form a wide variety of noncovalently bonded, solvent-shielding mesomorphic structures in aqueous solution. This emergent cooperative phenomenon, usually termed self-assembly, arises from solute−solvent hydrophobic interactions,[2] and it is morphologically restricted by geometric constraints.[3] The formed nanoaggregates offer hydrophobic microdomains inside of the solution that allow the location of solvophobic moieties. These facts, together with their ability to bind to polymers and macromolecules in solution, are responsible for the extreme importance of amphiphilic molecules in many scientific and industrial areas ranging from oil recovery to efficient delivery of drugs or complexation with biopolymers.

With the advent of modern ILs, a whole category of complex solvents has appeared comprising a huge number of members (it has been estimated to be around 10^{18}).[4] Moreover, given their ability to undergo multiple solvation interactions with many molecules, the emergence of research interest on the formation of nanostructured aggregates of surfactants in IL solution was just a question of time. Surfactant organization in ILs could open new trends toward catalysis, gelification, or lyotropic properties. In fact, this interest can be traced back to the work of Evans et al. in the early 1980s,[5] in which the authors analyzed the occurrence of micellar-like aggregates of the *n*-alkyltrimethylammonium family (n = 14, 16) in a protic IL, EAN. By means of light scattering measurements, they observed the formation of spherical micelles of the amphiphilic molecules in EAN and reported critical micelle concentrations (CMCs), micellar aggregation numbers, second

Received: April 6, 2011
Revised: May 23, 2011
Published: June 07, 2011

virial coefficients, and hydrodynamic radii. This was indicative of the structuring of the solvent around nonpolar groups in solution, a fact previously suggested by the observation of negative enthalpy and entropy changes upon the transference of rare gases and hydrocarbon moieties from cyclohexane to EAN.[5]

Despite the extreme interest of this topic, the 80s and 90s registered very little activity in it, and it was not until the past decade that some results started to be reported again on the promotion of self-assembly in both protic and aprotic ILs.[6−12] Contrary to the latter, the former are capable of forming hydrogen-bonded networks, and therefore, they are susceptible to supporting amphiphilic self-assembly. However, amphiphilic self-assembly nanostructures have also been observed recently in aprotic ILs. Anderson et al.[6] reported solvophobic interactions of ILs with the hydrophobic part of surfactants by means of measurements of the surface tension of surfactant solutions in aprotic 1-butyl-3-methylimidazolium chloride and hexafluorophosphate. Patrascu et al.[7] and Fletcher and Pandey[8] also showed that the formation of a micellar phase in aprotic ILs is possible, despite the absence of a hydrogen-bond network. The size and aggregation number of the formed micelles are tunable by changing the exact nature of the IL. Moreover, the formation of micelles of long-chain ILs in aprotic ILs of the imidazolium family has been reported.[9] However, definitive proof of the existence of micelles in aprotic IL solutions is still lacking, to our knowledge. In Araos and Warr words:[10] "Although there is mounting evidence in favor of self-assembling by small surfactant molecules in imidazolium and related ionic liquids, micelles have not been unambiguously shown to exist."

This is not the case for protic ILs like EAN, according to the same authors,[10] who consider that the formation of micelles in this IL was already proven in the 80s. In 2006, Velasco et al.[11] reported the formation of micelles of alkylammonium nitrates in EAN at room temperature. These authors reported CMCs for four different compounds experimentally determined using surface tension measurements, and they analyzed the effect of micelle formation on the partial molar volume of EAN, concluding that no change in this magnitude is registered upon micellization. Hence, contrary to what happens in water, the self-assembly process seems to provoke no change in the solvent structure. The main differences between amphiphilic association in room-temperature ILs and that in water were reviewed by Hao et al. in 2008.[12] Araos and Warr themselves[10] systematically explored the formation of micelles of polyoxyethylene surfactants in EAN and related the observed properties to their homologues in aqueous solutions. Surfactant self-assembly in protic ionic liquids has also been extensively treated by Drummond and co-workers in the past decade, who reported recently the self-assembly behavior of several surfactants in different protic ionic liquids,[13−15] and extensive reviews on this trending topic.[16,17]

Nevertheless, many efforts must still be devoted to the analysis of the phenomenology of formation and the structure of micelles in EAN and other protic ILs in order to have an idea similar to the one that we have for aqueous solutions. Particularly, we must know the dependence of the CMC on the amphiphilic chain length, size and shape of the micelles, the thermodynamics of micellization, and so forth. Moreover, very limited attention seems to have been devoted to the effect of the chain length of the IL solvent on the self-assembly of amphiphilic moieties. This effect is clearly nonobservable in water and other nonaqueous solvents, in which the solvophobic degree is fixed, but it is extremely important for ILs given the large number of possible solvents in this category. In this sense, Atkin et al.[18] recently investigated the phase behavior and self-assembled microstructures of several oligo(oxyethylene)-*n*-alkyl ether surfactants in propylammonium nitrate (PAN). These authors analyzed the effect of using this IL instead of EAN on amphiphilic self-assembly in micelles and liquid crystals (binary systems) and microemulsions (ternary systems). However, as far as we know, no systematic comparison of the main features of the self-assembly of surfactants in both solvents has been reported up to now.

In this paper, we report a study of the CMCs, size distributions, and thermodynamics of micellization of *n*-alkyltrimethylammonium (C_nTAX) and *n*-alkylpiridinium (C_nPyrX) halides (X = Br, Cl) in EAN and PAN, and we analyze the influence of the chain length of both solute and solvent cations and that of the surfactant anion on those properties.

2. EXPERIMENTAL SECTION

Chemicals. Ethylammonium nitrate and propylammonium nitrate were purchased from IOLITEC with purity degrees > 97 and 98%, respectively, and they were used as received. All of the surfactants used in this study were from Sigma Aldrich, and all of them were used as received. Their purity degrees are as follows: decyltrimethylammonium bromide (>98%), dodecyltrimethylammonium bromide (∼99%), tetradecyltrimethylammonium bromide (99% aprox.), hexadecyltrimethylammonium bromide (>98%), dodecyltrimethylammonium chloride (>99%), tetradecyltrimethylammonium chloride (>98%), dodecylpyridinium chloride (98%), hexadecylpyridinium chloride (99%), and hexadecylpyridinium bromide (99%). All samples were prepared by weight, by dilution of a concentrated solution, except in the case of the more concentrated solutions, which were individually prepared. The concentrations are expressed in molality.

Surface Tension Measurements. The surface tension of our systems was measured by means of a pendant drop Langmuir-type balance. The whole setup including image capturing, microinjectors, the axisymmetric drop shape analysis (ADSA) algorithm, and a fuzzy pressure control was managed by a Windows integrated program (DINATEN) and has been described elsewhere.[19] However, in our case, the solution droplets were formed manually at the tip of a capillary due to the great viscosity of our systems. The drop profiles were automatically transformed into physical coordinates and fitted to the Young−Laplace equation of capillarity by using ADSA, the liquid density difference and the local gravity being the only inputs. The drop volume, V, the interfacial tension, γ, and the surface area, A, were then numerically calculated finding the parameters that optimize the experimental pendant drop shape. This was done by minimizing the error function defined by the normal distances between the experimental drop and the theoretical predictions of Young−Laplace equations. Numerical integration was performed by combining a fourth-order Rung−Kutta method and a Newton−Raphson method. A good fitting was considered to be achieved when the absolute error was below 10^{-9}. The drop area was controlled by means of a modulated fuzzy logic PID (proportional, integral, and derivative control) algorithm. During the experiment, the drop was immersed in a thermostatted and vapor-saturated standard spectrophotometer aluminum cuvette (Hellma), minimizing contamination and drop evaporation. The setup was placed on a pneumatic vibration-damped optical bench table in a clean environment. All experiments were performed at (25.0 ± 0.1) °C, controlled by a

thermostat bath with recycling water. The obtained results were highly reproducible; each measurement was repeated at least 10 times with drops of size > 10 μL, and the average was then calculated. The standard deviations on γ and A were estimated to be $\pm$0.01 mJ m^{-2} and $\pm$0.005 nm^2 molecule^{-1}, respectively.

Transmission Electron Microscopy. TEM sample preparation and image acquisition procedures followed in this work have been described elsewhere.[20] In brief, samples were applied to carbon-coated copper grids, blotted, negatively stained with 2% (w/v) phosphotungstic S5 acid, air-dried, and then examined with a Phillips CM-12 electron microscope operating at an acceleration voltage of 120 kV. Neither dilution nor addition of more than one drop to the grid was needed for any sample. After preparation, samples were left for incubation overnight prior to imaging. All experiments were carried out at room temperature.

Dynamic Light Scattering (DLS). DLS measurements were performed using a setup designed by ALV, which included, among others, a neutral filter, a photodiode, polarizing prisms, and a set of pinholes. The photodiode at the incoming beam allowed permanent sampling of the intensity (of light entering the cell). The sample temperature was maintained at 25 °C by a thermostat with an accuracy of $\pm$0.005 °C. The intensity autocorrelation function was obtained by applying an ALV-5000 correlator card with a 400 mW solid-state laser from Coherent (Model 532-420) operating at 532 nm. All of the measurements were made at an angle of 90°.

Electrochemical Measurements. The cationic surfactant-selective electrode was prepared in the laboratory, as described previously.[21,22] This electrode was made with a plasticized poly(vinylchloride) (PVC) membrane containing 20 wt % PVC, 80 wt % dinonylphtalate (the plasticizer), and, as the carrier, dodecylpyridinium or hexadecylpyridinium tetraphenylborate salts for dodecylpyridinium- or hexadecylpyridinium-selective membranes, respectively. The surfactant-selective electrode was combined with a KCl-saturated calomel reference electrode protected from amphiphile diffusion by a saline gel made of 2 mol L^{-1} KNO_3 in agar−agar.

internal reference	aqueous solution of surfactant 10^{-3} mol L^{-1}	selective membrane	surfactant in IL	external reference

Surfactant-selective electrode

The emf of this cell in the IL can be written as

$$\Delta E = \text{constant} + S \ln a_{M^+} \quad (1)$$

in which a_{M^+} is the surfactant activity in the IL and S is the slope of the electrode response. When the M^+ concentration is smaller than that of the IL, the activity coefficient of M^+ is constant (because the ionic strength is fixed by the IL) and can be included in a constant term. The emf is then directly related to the M^+ concentration in the IL

$$\Delta E = \text{constant}' + S \ln[M^+] \quad (2)$$

The emf values of this cell, measured with a millivoltmeter (Radiometer PHM250), were stable within $\pm$0.3 mV for a few seconds and reproducible within $\pm$0.5 mV. All measurements were carried out at 298.0 $\pm$ 0.1 K.

3. RESULTS AND DISCUSSION

The densities of pure EAN and PAN at room temperature (demanded by our previously described fitting procedure for the surface tension) were taken to be ρ_{EAN} = 1.2016 g cm^{-3},[13] and ρ_{PAN} = 1.1570 g cm^{-3},[23] respectively. In Figure 1, we show the surface tension of C_nTABr (n = 10, 12, 14) in EAN (Figure 1a), C_nTACl (n = 12, 14) in EAN (Figure 1b), and C_nTABr (n = 12, 14, 16) in PAN (Figure 1c). The CMC was obtained by means of the Williams method in all cases; therefore, it was identified with the concentration at which the two straight lines of the property above and below the CMC intersect. As can be observed, typical markedly steep decreases in the surface tension are initially registered in all cases, followed by a transition to an almost constant asymptotic value of this magnitude. As is well-known from self-assembly processes in aqueous solutions, this behavior is associated with the formation of an amphiphilic monolayer in the free air−IL interface that decreases the surface tension of the pure ILs. Once this interface is saturated by surfactant molecules, at a more or less well-defined concentration known as the CMC, self-assembly micellar nanoaggregates start to form in the bulk IL solution, and the surface tension at the free surface of the solution does not suffer any additional change. Of course, this process of nanostructuration of the IL−surfactant solution is driven by a solvophobic effect that induces the association of the surfactant molecules in order to minimize contacts with the IL. As is also the case in aqueous solutions, the CMC decreases with the alkyl chain length of the amphiphilic molecule, but the registered values are considerably greater (approximately 1 order of magnitude) than those in the corresponding aqueous solutions (see Table 1). This clearly indicates that the intensity of the surfactant−solvent lyophobic interactions is much lower in ILs than that in water. Our results are compatible with those reported by Evans et al.[5] and also by Velasco et al.[11] for the same family of surfactants.

In Figure 1a, one can also see that lower values of the saturation surface tension of C_nTAB are registered for increasing chain length, in agreement with the behavior in aqueous solutions. In this sense, it is remarkable that the saturation surface pressures $\pi = \gamma - \gamma_{min}$ are very similar for C_{12}TABr and C_{14}TABr (approximately 10 and 11 mN m^{-1}, respectively) but only 8 mN m^{-1} for C_{10}TABr. In some of the studied cases, a slow decrease of the surface tension is registered at concentrations above the CMC, but this tendency is reduced as the surfactant chain length increases. Finally, we point out that the value of this difference in surface pressure in water solutions is considerably greater for these compounds (around 35 mN m^{-1} according to Moulik et al.[29]).

Next, we consider the effect of the surfactant counterion in the micellization of surfactants in ILs. It is well-known that the counterion stabilizes ionic surfactant micelles in aqueous solution by binding to the micelles and screening the electrostatic repulsions between head groups, and consequently, the binding affinity of the counterion must influence the process of micellization. It has been previously shown that the counterion has a strong effect on the thermodynamics and aggregation properties of micellization in water (see ref 30 and references therein). The effect of monovalent counterions on the CMCs of surfactants in aqueous solution has been reported to follow the Hoffmeister

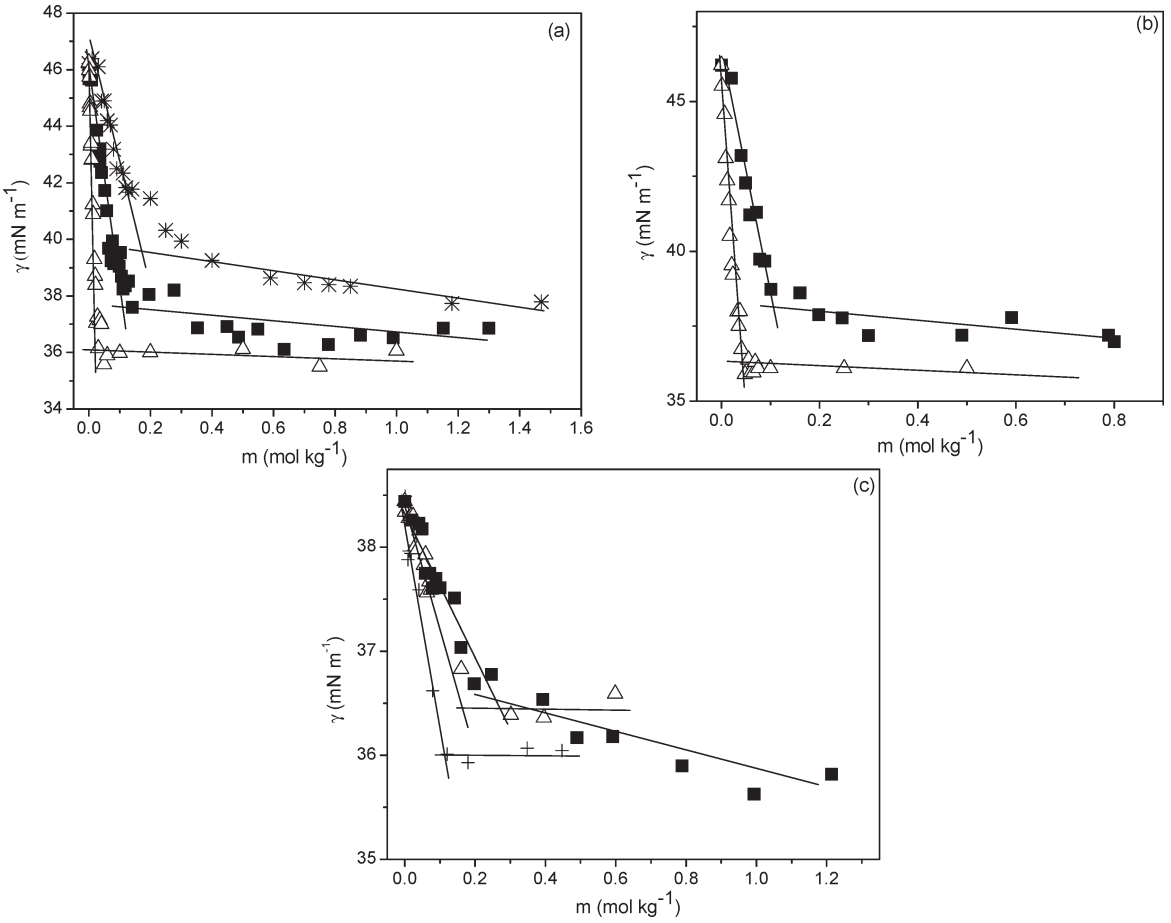

Figure 1. Concentration dependence of the surface tension of (a) C_nTABr in EAN, (b) C_nTACl in EAN, and (c) C_nTABr in PAN at 25 °C. The symbols correspond in all cases to the following chain lengths: (∗) n = 10, (■) n = 12, (△) n = 14, and (+) n = 16. The lines are guides to the eye.

Table 1. Critical Micelle Concentrations (CMCs) of the Analyzed Compounds at 25 °C Obtained from Surface Tension Measurements

	CMC_{EAN} (mol kg^{-1})	CMC_{PAN} (mol kg^{-1})	CMC_{water} (mol kg^{-1})
C_{10}TABr	0.174 ± 0.040		0.0602[24]
C_{12}TABr	0.100 ± 0.010	0.26 ± 0.10	0.0133[25]
C_{14}TABr	0.0249 ± 0.0037	0.161 ± 0.050	0.00341[25]
C_{16}TABr		0.113 ± 0.012	0.001[25]
C_{12}TACl	0.105 ± 0.032	–	0.00226[26]
C_{14}TACl	0.0330 ± 0.0060	–	0.00447[27]
C_{12}PyrCl	0.100 ± 0.010	0.293 ± 0.061	0.0112[28]
C_{16}PyrCl	0.01270 ± 0.000050	0.100 ± 0.024	0.00097[28]

series.[30] The position of an anion in this series is normally considered to depend on its hydrated radius.[31] A smaller hydrated radius enhances the ability of the anion to bind at the micellar surface, which decreases the electrostatic repulsion between the surfactant head groups and hence favors aggregation, lowering the CMC and the degree of ionization, α. In order to test this behavior in an IL solution, in Figure 1b, we present the concentration dependence of the surface tension of *n*-alkyltrimethylammonium chlorides (C_nTACl, n = 12, 14), and the corresponding CMCs are listed in Table 1 for EAN, together with their reported values for aqueous solution. As expected, small changes are registered with respect to their counterparts with a bromide anion. However, the CMCs of the surfactants with a chloride counterion are a little bit greater than the ones shown by those with a bromide anion in their molecular structure. This could suggest that chloride anions are also more strongly solvated in ILs than their bromide homologues, similarly to what happens in water (hydrated radii: r_{Cl^-} = 3.32 Å, r_{Br^-} = 3.30 Å).[31] However, the high concentrations of anions in these systems (coming from both the IL (NO_3^-) and the surfactant itself) prevent us from concluding that this behavior is only a responsibility of the surfactant anion. In fact, NO_3^- is present in a much higher proportion than that of the surfactant anion. However, what one can conclude from the experimental evidence is that Br^- seems much more capable of replacing the biggest NO_3^- anion in the micellar surface than Cl^-, thus favoring the formation of micelles at lower concentrations. However, further work is necessary in order to clearly establish the role of the surfactant anion in self-assembly processes in ILs.

The effect of chain length of the IL solvent is analyzed in Figure 1c, where we represent the dependence of the surface tension of C_nTABr (n = 12, 14, 16) in PAN. We have selected two extreme cases, one of short chain length (in this respect, it must be stated that the results for C_{10}TABr were not conclusive in this solvent) and the one with the longest chain length employed in this paper. As can be seen in this representation,

dx.doi.org/10.1021/jp203204c |J. Phys. Chem. B 2011, 115, 8145–8154

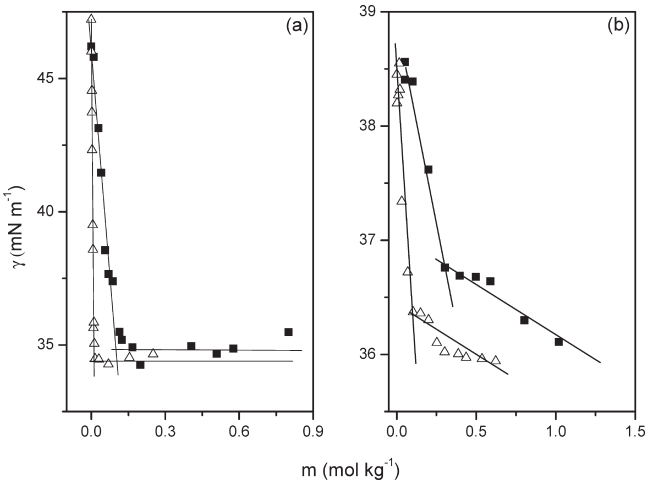

Figure 2. Concentration dependence of the surface tension of (■) dodecyl and (△) hexadecylpyridinium chlorides in EAN (a) and PAN (b) at 25 °C.

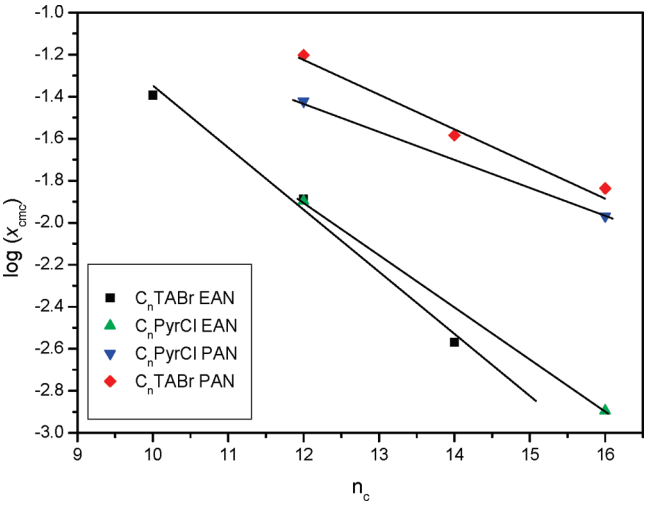

Figure 3. Dependence of the logarithm of the CMCs of the studied surfactants in EAN and PAN on the number of carbon atoms in the alkyl chain length of the surfactant cation. The lines correspond to the fitting to a Stauff−Klevens-type law, except for those of the pyridinium family, which are mere guides to the eye.

both compounds exhibit CMCs at concentrations that follow the same trend observed in EAN (see Table 1), the longer the alkyl chain length of the surfactant, the lower the critical aggregation concentration. Moreover, it is interesting to note that the CMCs of these surfactants in PAN are approximately an order of magnitude higher than those in EAN, suggesting a much lower solvophobic effect in this IL. This fact is also reflected in the values of the slopes of the surface tension data above the CMC for C_{12}TABr in both cases.

Finally, where tensiometry of solutions of surfactants in EAN is concerned, we consider the influence of the head group of the surfactant on the micellization behavior. Figure 2a shows the behavior of the surface tension of *n*-alkylpyridinium chlorides (n = 12, 16) with the concentration in EAN. The values of the CMCs are once more contained in Table 1. One can observe in both cases the typical behavior of the surface tension of an amphiphilic substance in a solvent; therefore, once more, the formation of self-assembly aggregates is confirmed in both solvents. Surprisingly enough, we observe that the presence of the pyridinium group in the amphiphilic molecular architecture provokes no clear difference in the aggregation behavior in EAN and PAN of surfactants of this family with respect to those with the alkyltrimethylammonium group. This suggests that the solvophobic interactions of the pyridinium group with both protic solvents are very similar to those of the alkyltrimethylammonium group, despite the fact that the latter shares a part of its molecular structure with the protic solvents. This indicates that the alkyl chain length of the surfactant must be mainly responsible for the solvophobic incompatibility of the surfactant with these protic ILs. This will be confirmed in the following through the analysis of the CMC on the number of carbon atoms in the molecular structure of the surfactant.

As is well-known, the logarithm of the CMC in aqueous surfactant solutions shows a linearly decreasing behavior of the logarithm of the molar fraction of the system at its CMC (x_{CMC}) with the number of carbon atoms in the hydrophobic chain, in what constitutes the basis of the so-called Stauff−Klevens equation (see ref 28 and references therein)

$$\ln x_{CMC} = A - Bn_C \qquad B > 0 \tag{3}$$

where n_C is the number of carbon atoms in the monomer chain and A and B are usually treated as adjustable parameters. The above semiphenomenological result applies to the formation of self-assembled nanostructures of amphiphiles held together by noncovalent interactions, and it is a consequence of the growth of the solvophobicity of the chain with an increase in the number of alkyl groups in its molecular structure. Figure 3 shows the dependence of the CMC with the number of carbon atoms in the alkyl chain of the surfactant for our surfactant solutions in ILs, and we can clearly observe that a linear trend is registered in all of the studied cases. We have fitted our experimental results to eq 1, and the value obtained for the slope of the alkyltrimethylammonium bromides in EAN was B = 0.29, similar although a little bit smaller than that for long-chain monovalent amphiphiles in water, B = 0.31−0.32, which means that the CMC decreases approximately by a factor of 4 when the number of methylene groups in the alkyl chain is doubled.[32] This family shows an even smaller value of the slope in PAN, B = 0.159, due to the smaller solvophobicity of this solvent. However, what is clearly shown in this representation is that the value of A suffers considerable change with the solvent, being A = 1.58 for surfactants in EAN and A = 0.58 in PAN. In the case of the pyridinium family, the difficulty in purchasing C_{14}PyrCl for this paper implied that we could obtain only two points; therefore, a proper linear fit was not possible. However, the slopes qualitatively calculated with the points shown in Figure 3 suggest that these values could be approximately B = 0.25 in EAN and B = 0.14 in PAN. Evans et al.[5] reported similar results for alkyltrimethylammonium and alkylpyridinium surfactants in EAN at 50 °C, confirming the Stauff−Klevens law with B = 0.25 for both families and A = 1.40 for the former and A = 0.149 for the latter. Our results are highly compatible with these within the limits of the experimental uncertainty.

In Table 2, we present the Gibbs free energy of micellization calculated using the well-known mass action model

$$\Delta G^0_{mic} = (2 - \beta)RT \log x_{CMC} \tag{4}$$

where β is the ionization degree of the micelle, which can be taken to be β = 1 due to the exclusively ionic shell surrounding the aggregates in ILs. On the other hand, x_{CMC} is the molar

Table 2. Gibbs Free Energy of Micellization and Area Per Monomer at 25 °C Obtained Using the Gibbs Adsorption Isotherm for the Surfactants Employed in This Work[a]

	EAN		PAN		water	
	ΔG_{mic} (kJ mol^{-1})	A_{min} (nm^2)	ΔG_{mic} (kJ mol^{-1})	A_{min} (nm^2)	ΔG_{mic} (kJ mol^{-1})	A_{min} (nm^2)
C_{10}TABr	−9.70	1.49	−7.73	–	–	–
C_{12}TABr	−10.77	1.13	−8.53	8.42	−18.4[29]	1.18[29]
C_{14}TABr	−14.67	0.80	−9.82	7.00	−25.3[29]	0.72[29]
C_{16}TABr	−15.83	–	−10.62	5.39	−30.5[29]	1.48[29]
			–	–		
C_{12}TACl	−11.11	0.95			−31.5[33]	
C_{14}TACl	−14.13	0.97	–	–	−37.6[33]	
					−32.6[34]	
C_{12}PyCl	−11.23	0.93	−8.26	4.90	−31.19[35]	0.53[36]
C_{16}PyCl	−16.52	0.73	−10.92	4.12	−28.2[29]	0.71[29]

[a] Results of ref 29 were obtained at 303 K.

fraction of the solution at the CMC. Moreover, this table contains also the minimum area per surfactant molecule at the air−solvent interface calculated using the conventional Gibbs adsorption isotherm

$$A_{min} = 1/N_A\Gamma_{max}$$
$$\Gamma_{max} = -\frac{1}{\nu RT}\left(\frac{\partial\gamma}{\partial \ln c}\right)_{T,P} \quad (5)$$

where ν represents the number of ions per surfactant molecule (two in our case), R is the gas constant, N_A is Avogadro's number, and Γ_{max} is the maximum surface excess concentration of the surfactant. As one can observe in Table 2, the values of ΔG^0_{mic} follow the same trend in EAN and PAN as they do in water, increasing with alkyl chain length. However, the calculated values are notably lower in the case of EAN with respect to water and of PAN with respect to EAN, reflecting once more the influence of the solvophobic effect in the energetics of the nanoaggregation. Particularly, in no case is the typical value of the Gibbs free energy of micellization per methylene group of ionic and nonionic surfactant in water at 25 °C, −2.84 kJ,[5] reached. The free energies of transfer of a methylene group from the IL to the micelle interior are calculated to be −0.973 kJ mol^{-1} in EAN and −0.691 kJ mol^{-1} in PAN.

On the other hand, where the area per monomer is concerned, once more we observe in Table 2 the same trends; the minimum areas per monomer, A_{min}, decrease with the increase of the alkyl chain length, except perhaps for C_nTACl, in which no conclusive results were obtained in this work. The values in PAN are significantly higher than those in EAN, being in both cases higher than those in water. This reflects once more a weaker adsorption at the air−IL interface of the surfactant, in agreement with our previous observation for the surface tension decrease above the CMC.

As mentioned previously, we have also performed negative-staining TEM observations of the surfactant solutions analyzed in this paper. As an example of the obtained results, we show images for C_{12}TABr in EAN in Figure 4. Here, spherical aggregates at concentrations above the CMC can be observed, whose radii are shown in Table 3. In this case, it is very clear that while below the CMC, no micellar aggregate is observed

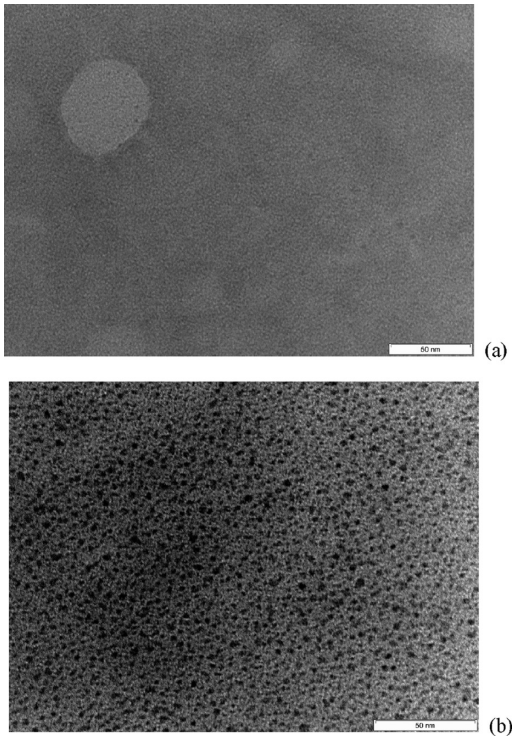

Figure 4. TEM images of C_{12}TABr in EAN at concentrations of (a) m = 0.04 mol kg^{-1} < CMC and (b) m = 0.5 mol kg^{-1} > CMC. The scale bars represent 50 nm in both cases.

(although something like a vesicle seems to appear in the shown picture, but further confirmation is needed), and at concentrations above the CMC, self-association aggregates of the surfactant are clearly visible in great number in the bulk solution. The same behavior was also registered in all of the other studied compounds in EAN and PAN, in agreement with the surface tension observations. Figure 5 represents the TEM results for C_nTABr solutions in the studied ILs, and the results clearly confirm the formation of micelles. However, in this case, we detected a great morphological variety of structures, ranging from clusters of spherical micelles for C_{14}TABr at 0.40 mol kg^{-1} (b) to crystals at the highest

dx.doi.org/10.1021/jp203204c |J. Phys. Chem. B 2011, 115, 8145–8154

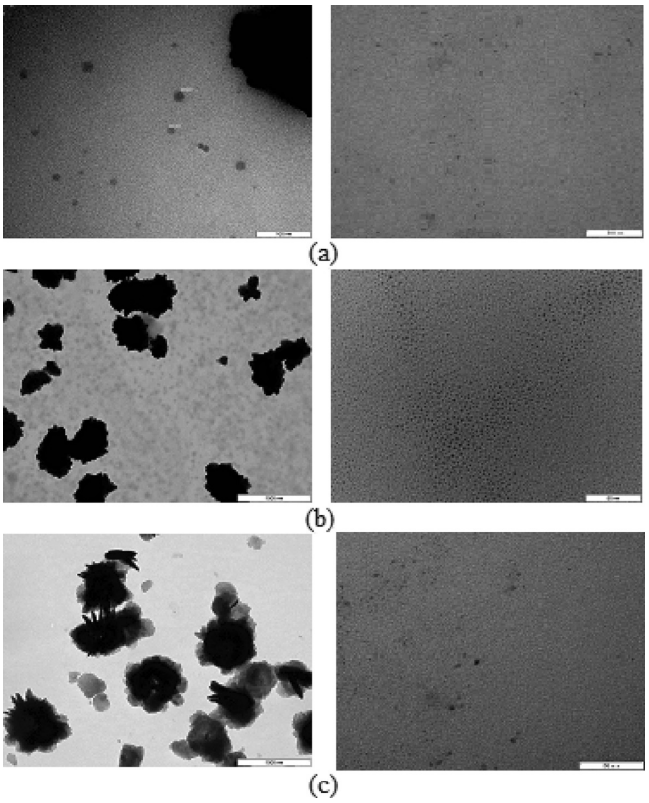

Figure 5. TEM images of alkyltrimethylammonium bromides in PAN at concentrations above the CMCs. (a) C_{12}TABr at m = 0.79 mol kg^{-1}, (b) C_{14}TABr at m = 0.40 mol kg^{-1}, and (c) C_{16}TABr at m = 0.12 mol kg^{-1}. The scale bars on the right represent 50 nm in all cases, 100 nm for the left image in (a), and 1000 nm for images on the left in (b) and (c).

Table 3. Size and Aggregation Number of Alkyltrimethylammonium Bromides in EAN and PAN at Several Concentrations above the Corresponding CMCs

	m (mol kg^{-1})	r (nm)	N_{agg}
C_{10}TABr (EAN)	0.48	1.16 ± 0.47	19 ± 15
C_{10}TABr (EAN)	1.47	1.36 ± 0.39	36 ± 30
C_{12}TABr (EAN)	0.50	1.51 ± 0.61	38 ± 26
C_{14}TABr (EAN)	0.026	1.90 ± 0.75	53 ± 35
C_{12}TABr (PAN)	0.79	1.11 ± 0.43	18 ± 15
C_{14}TABr (PAN)	0.40	1.21 ± 0.42	22 ± 16

surfactant concentrations employed in these measurements. Interestingly enough, these lyotropic liquid crystals have also been reported for oligo(oxyethylene)-*n*-alkyl ether surfactants with hexadecyl chains or longer in PAN by Atkin et al.,[18] but to our knowledge, they have never been directly observed previously, neither for trimethylammonium nor any other surfactant in this solvent.

We used the particle detection features in the ImageJ image analyzing software[37] to obtain a precise estimate of the sizes of the formed micelles in the bulk IL solutions. In Figure 6, we represent the radius histograms for all of the studied cases together with the associated optimal bandwidth kernel density estimates obtained using the R statistical package.[38] To obtain the distributions of aggregation numbers from this data, we used the standard expression[5]

$$V = \frac{4}{3}\pi r^3 = (27.4 + 26.9n_C)N_{agg} \quad (6)$$

where it is assumed that 27.4 and 26.9 are the volumes in Å^3 of the methyl and methylene groups respectively.[5]

The resulting distributions have been fitted to both Gaussian and Schultz functional forms following a maximum likelihood criterion. The Schultz distribution of parameter p and mean $\langle s\rangle$ for the aggregation number s reads

$$f(s) = \frac{(p+1)^{p+1}s^p}{\Gamma(s+1)\langle s\rangle^{p+1}}e^{-(p+1)s/\langle s\rangle} \quad (7)$$

where $\Gamma(n) = (n-1)!$ stands here for the Euler gamma function. The above is just an alternative expression for the well-known gamma distribution. It is asymmetric, it belongs to the exponential class of distributions, and it has been reported to accurately describe polydispersed droplets of three-component microemulsions.[39] The predictions of this distribution for C_{12}TABr in PAN are shown in Figure 7, where it is visible that it fits the experimentally observed kernel density more accurately than the Gaussian distribution. The numeric results for the average sizes and aggregation numbers and those for their mean-squared deviations (polydispersities) afforded by the best-fit Schultz distribution are shown in Table 3. It is visible in Table 3 that the aggregation numbers of surfactants in EAN are considerably larger than those in PAN and that very high values for the dispersion of the aggregation numbers are obtained. Moreover, as pointed out by Evans et al.,[5] the maximum length of a fully extended chain can be estimated from $l_C = 1.5 + 1.265n_C$ and gives values of 17, 19, and 22 Å for C_{12}TABr, C_{14}TABr, and C_{16}TABr, respectively. Thus, given that the values of the radii in Table 3 imply $r/l_C < 1$, many of the surfactant chains must be folded in the bulk micellar core; therefore, the terminal methylene groups are located near the micellar interfaces. This tendency is more markedly observed in PAN than in EAN.

We also performed DLS measurements in IL solutions of the surfactant of the pyridinium family but only for the compound with the longest alkyl chain of those considered. Attempts to obtain DLS measurements for other surfactants in EAN or PAN were unsuccessful, probably due to the closeness of the refractive indexes of surfactants containing only a saturated hydrocarbon chain to that of the solvents; therefore, the excess intensity of light scattered by micelles is too small to be observed.[5] The other compounds exhibit spurious correlations that prevented us from obtaining clearly determined correlation functions. These measurements were made at 30 °C to ensure that we were sufficiently beyond the Krafft point, below which no micellar aggregate can exist. The results for the intensity autocorrelation functions, $g_2(\tau)$, of C_{16}PyrCl in EAN and PAN are shown in Figure 8, in both cases for concentrations below and above the CMC. One can see in these correlograms that the formation of micelles is accompanied by a notable increase in the correlation reflecting the formation of nanoparticles in the bulk solutions. This definitively demonstrates the occurrence of a cooperative self-assembly process controlled by the surfactant concentration.

From these results, we can obtain the diffusion coefficients of the nanoaggregates using the well-known CONTIN method.[40]

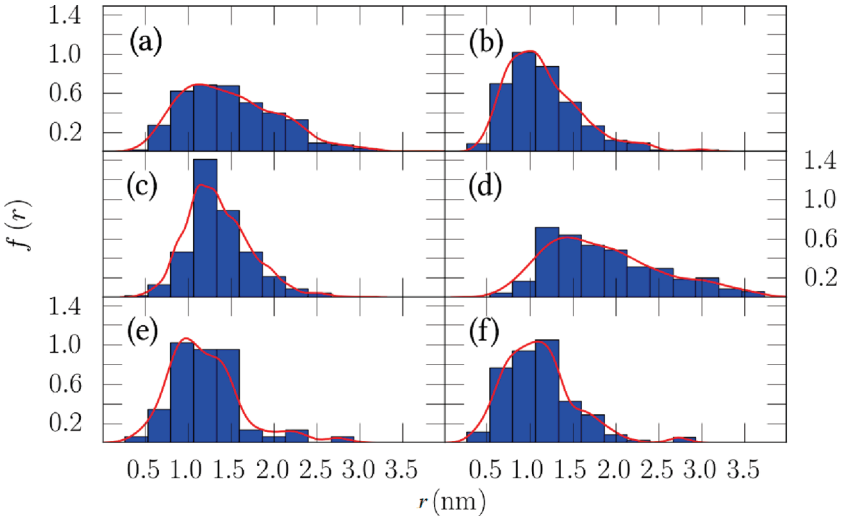

Figure 6. Histograms and kernel density estimates (red line) of radii for (a) C_{10}TABr in EAN at m = 0.48 mol kg^{-1}, (b) C_{10}TABr in EAN at m = 1.47 mol kg^{-1}, (c) C_{12}TABr in EAN at m = 0.50 mol kg^{-1}, (d) C_{14}TABr in EAN at m = 0.026 mol kg^{-1}, (e) C_{12}TABr in PAN at m = 0.79 mol kg^{-1}, and (f) C_{14}TABr in PAN at m = 0.40 mol kg^{-1}.

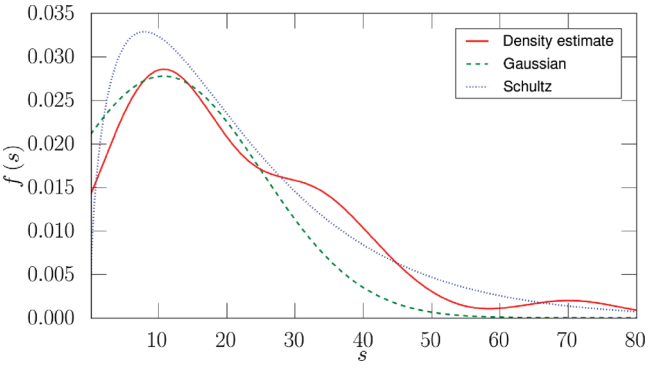

Figure 7. Kernel density estimate with optimal bandwidth of the distribution of aggregation numbers for C_{12}TABr in PAN at m = 0.79 mol kg^{-1} (solid line) along with maximum likelihood fits of the experimental data to Gaussian (dashed line) and Schultz (dotted line) distribution functions.

In brief, this method uses the field correlation function given by the Siegert equation

$$g_1(\tau) = \sqrt{g_2(\tau) - 1} \tag{8}$$

and relates it to the diffusion coefficients for the particles of a polydisperse system assuming exponential decay of each species present; therefore

$$g_1(\tau) = \int_{\chi_{min}}^{\chi_{max}} G(\chi) e^{-\chi\tau}\, d\chi \tag{9}$$

Here, G(χ) is the distribution function of the decay rate, $\chi = Dq^2$, with

$$q = \frac{4\pi n}{\lambda} \sin\theta \tag{10}$$

being the scattering vector, n the refractive index, λ the radiation wavelength, and θ the scattering angle. Numerically solving the above equation by standard procedures, we can obtain the diffusion coefficient of the particles in the bulk from the correlograms. Afterward, we calculate the hydrodynamic radius of the micelles in the bulk using the Stokes−Einstein equation for the diffusion coefficient

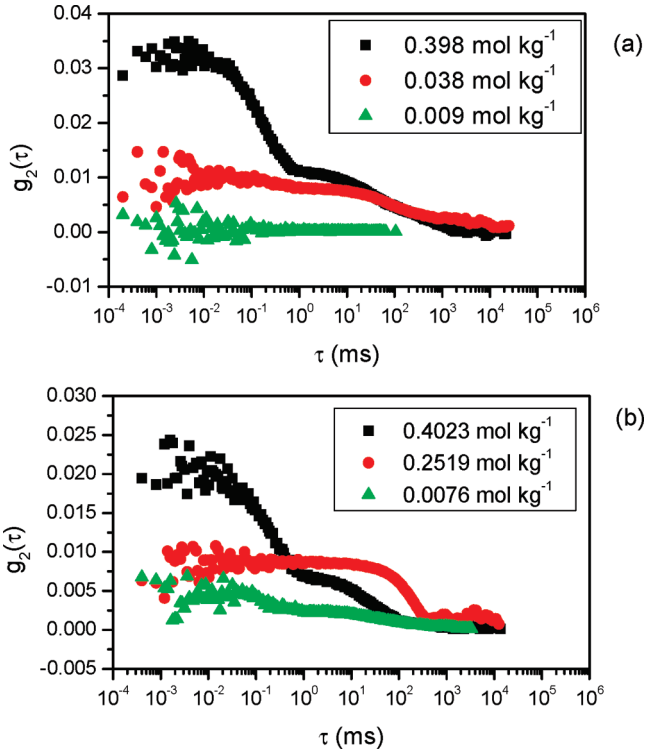

Figure 8. Intensity autocorrelation function of C_{16}PyrCl in (a) EAN and (b) PAN.

$$D = \frac{k_B T}{6\pi\eta r_H} \tag{11}$$

The results calculated for C_{16}PyrCl in EAN (η = 32 cP at 25 °C, n = 1.4524)[13] and PAN (η = 66.6 cP at 25 °C, n = 1.4561)[23] were

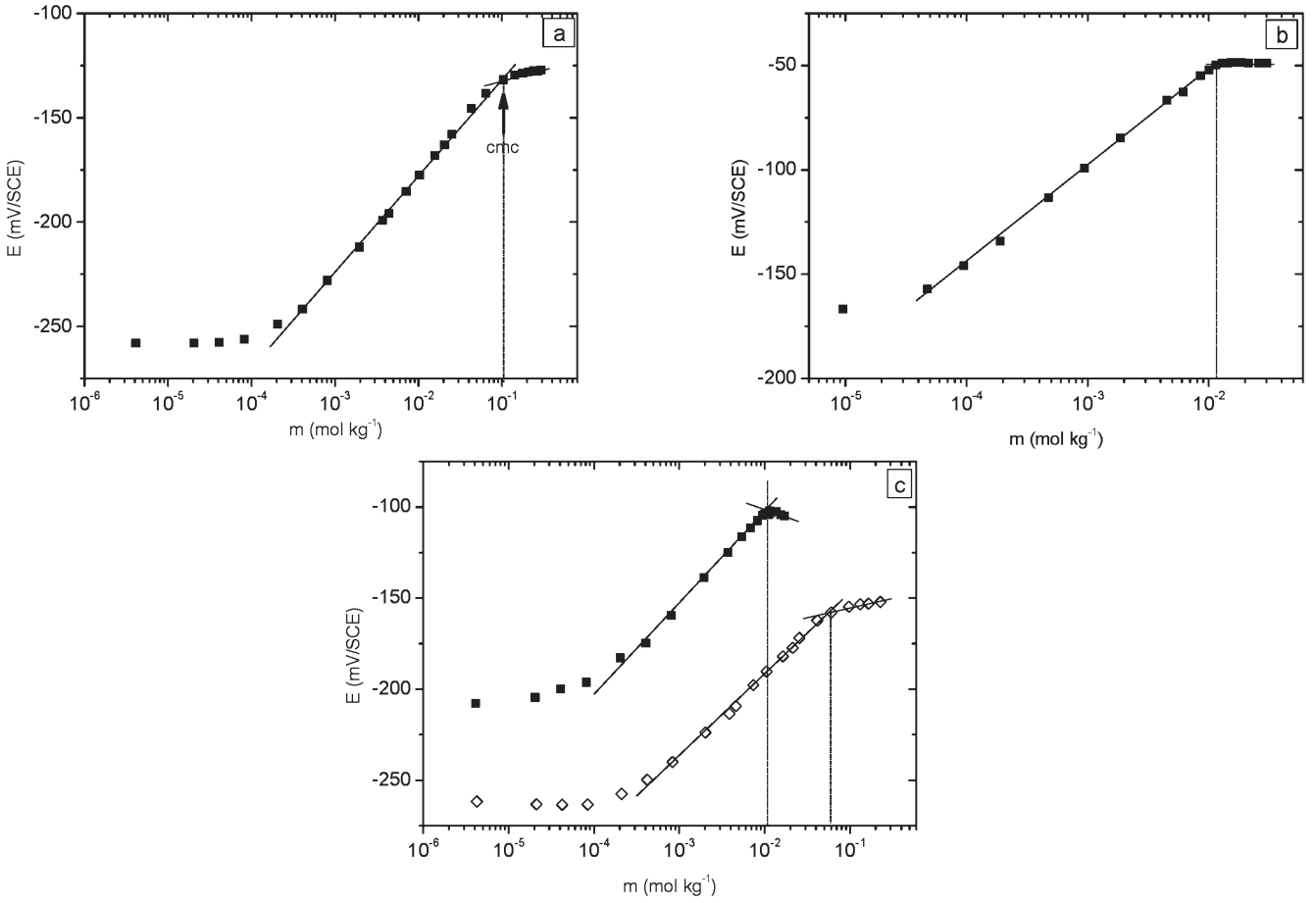

Figure 9. Variation of the ion-selective electrodes with the concentration of (a) C_{12}PyrCl in EAN, (b) C_{16}PyrCl in EAN, and (c) C_{16}PyrBr in EAN (dark squares) and in PAN (open diamonds) at 25 °C.

Table 4. CMCs of Alkylpyridinium Halides in EAN and PAN at 25 °C Obtained from Potentiometric Measurements

	CMC_{EAN} (mol kg^{-1})	CMC_{PAN} (mol kg^{-1})
C_{12}PyrCl	0.104 ± 0.010	
C_{16}PyrCl	0.0115 ± 0.0010	
C_{16}PyrBr	0.0106 ± 0.0010	0.0413 ± 0.0040

r_H = (1.49 ± 0.40) and (1.14 ± 0.33) nm, respectively. It is noteworthy that the calculated value for C_{16}PyrCl in EAN is in excellent agreement with that estimated by Evans et al.[5] of 1.42 nm and also, given the experimental uncertainties, with the radius evaluated as the sum of the sizes of the constituents of this molecule, 1.98 nm.

Finally, we used a surfactant-selective electrode to determine the CMCs of the studied compounds. This sensor follows the activity of the ionic surfactant in various media including ILs.[21,41] In Figure 9, we show the electromotive force of the electrochemical cell (comprised of the surfactant-selective electrode combined with the protected reference electrode) for C_nPyrCl (n = 12, 16) in EAN and C_{16}PyrBr in EAN and in PAN (Figure 9c). As can be seen, first, the potential increases linearly with the logarithm of the concentration. From a given concentration characteristic of a surfactant in a specific medium, a break point is observed. When micelles appear, the activity of free surfactants becomes constant. Thus, the break point corresponds to the CMC. The CMCs of C_{12}PyrCl and C_{16}PyrCl in EAN determined by potentiometry are in very good agreement with those obtained by tensiometry (see Table 4). We studied the effect of the counterions for C_{16}PyrX. As for the trimethylalkylammonium surfactants, we obtained a CMC for C_{16}PyrBr that was slightly lower than that for C_{16}PyrCl. Moreover, as for the other surfactants, the CMC of C_{16}PyrBr is four times higher in PAN than that in EAN.

4. CONCLUSIONS

We have experimentally observed the formation of nanostructures of surfactants of the families of the alkyltrimethylammonium and pyridinium families in two protic ILs, EAN and PAN, analyzing the role of the alkyl chain of both solute and solvent, as well as that of the surfactant counterion. We reported the surface tension of different members of these families in EAN and in PAN solutions, in the latter case for the first time, to our knowledge. We have evaluated the CMCs of these compounds in both solvents, the free energy of micellization in the mass action model, and the area per monomer in the air−IL interface, and we compared these magnitudes to those in aqueous solutions. Our results indicate that both in EAN and PAN solutions, the longer the solvent alkyl chain, the less favorable the process of micellization due to reduced difference in solvophobicity; therefore,

dx.doi.org/10.1021/jp203204c |J. Phys. Chem. B 2011, 115, 8145–8154

greater values of the CMCs are registered. Moreover, Br^- seems to favor micellization in a greater degree than Cl^-, which suggests that the former is more capable of replacing the anions of the IL in the surfactant aggregates than the latter. Surprisingly enough, there seems to be no appreciable difference between alkyltrimethylammonium and pyridinium behavior in these protic solvents, and very similar values of the analyzed magnitudes are registered in both cases, except for the minimum area per monomer in the air−IL interface. Moreover, we have directly observed by TEM the formation of aggregates of the analyzed magnitudes in EAN and, to the best of our knowledge, for the first time, in PAN. In this latter case, we observed the formation of lyotropic liquid crystal phases at high surfactant concentrations, in agreement with results previously reported in the literature. Using image analyzing software, we evaluated the size of the aggregates and their aggregation numbers, observing the same trends as those in water once again and detecting smaller aggregates as the solvophobicity of the solvent increased. DLS and electrode potential measurements confirmed the existence of amphiphilic self-assembly nanostructures in the bulk IL solution, and the CMC and aggregate size obtained with these techniques agree well with those obtained by means of the ones employed here.

Our observations indicate that the phenomenology of surfactant self-assembly in protic ILs is similar to that registered in water for the same surfactants. Consequently, our results are in essence compatible with the current consensus about the role of solvophobic interactions in the bulk solvent as the main feature responsible for the self-assembly processes in bulk IL solutions. All of our evidence suggests that, as is the case for water, the driving force of the self-assembly processes in protic ILs is the negative entropic contribution to the free energy of aggregation resulting from the release of the solvent-structured monolayer produced by limited solute−solvent hydrogen bonding and strong solvent−solvent interactions.

AUTHOR INFORMATION

Corresponding Author

* Tel: +34 881811000, ext. 13966. Fax: +34 881814112. E-mail: luismiguel.varela@usc.es.

ACKNOWLEDGMENT

The authors wish to thank the financial support of Spanish "Ministerio de Educación y Ciencia" under the Research Projects FIS2007-66823-C02-01 and FIS2007-66823-C02-02 and also the funding of Xunta de Galicia through the research projects of References 10-PXIB-103-294 PR and 10-PXIB-206-294 PR. All of these research projects are partially supported by FEDER funds. J.C. and T.M.-M. thank the Spanish Ministry of Education for their FPU grants.

REFERENCES

(1) Wilkes, J. S.; Zaworotko, J. *J. Chem. Soc., Chem. Commun.* **1992**, 965.
(2) Tanford, C. *The Hydrophobic Effect: Formation of Micelles and Biological Membranes*; Wiley: New York, 1980.
(3) Israelachvili, J. N.; Mitchell, D. J.; Ninham, B. W. *J. Chem. Soc., Faraday Trans. 2* **1976**, *72*, 1525–1568.
(4) Carmichael, A. J.; Seddon, K. R. *J. Phys. Org. Chem.* **2000**, *13*, 591–595.
(5) Evans, D. F.; Yamauchi, A.; Jason Wei, G.; Bloomfield, V. A. *J. Phys. Chem.* **1983**, *87*, 3537–3541.
(6) Anderson, J. L.; Pino, V.; Hagberg, E. C.; Sheares, V. V.; Armstrong, D. W. *Chem. Commun.* **2003**, 2444–2445.
(7) Patrascu, C.; Gauffre, F.; Nallet, F.; Bordes, R.; Oberdisse, J.; de Lauth-Viguerie, N.; Mingotaud, C. *ChemPhysChem* **2006**, *7*, 99–101.
(8) Fletcher, K. A.; Pandey, S. *Langmuir* **2004**, *20*, 33–36.
(9) Li, N.; Zang, S; Zheng, L.; Dong, B.; Li, X.; Yu, L. *Phys. Chem. Chem. Phys.* **2008**, *10*, 4375–4377.
(10) Araos, M. U.; Warr, G. G. *Langmuir* **2008**, *24*, 9354–9360.
(11) Velasco, S. B.; Turmine, M.; Caprio, D. D.; Letellier, P. *Colloids Surf., A* **2006**, *275*, 50–54.
(12) Hao, J.; Zemb, Th. N. *Curr. Opin. Colloid Interface Sci.* **2007**, *12*, 129–137.
(13) Greaves, T. L.; Weerawardena, A.; Fong, C.; Krodkiewska, I.; Drummond, C. *J. Phys. Chem. B* **2006**, *110*, 22479–22487.
(14) Greaves, T. L.; Weerawardena, A.; Fong, C.; Drummond, C. J. *Langmuir* **2007**, *23*, 402–404.
(15) Greaves, T. L.; Weerawardena, A.; Krodkiewska, I.; Drummond, C. J. *J Phys. Chem. B* **2008**, *112*, 896–905.
(16) Greaves, T. L.; Drummond, C. J. *Chem. Soc. Rev.* **2008**, *37*, 1709–1726.
(17) Greaves, T. L.; Drummond, C. J. *Chem. Rev.* **2008**, *108*, 206–237.
(18) Atkin, R.; Bobillier, S. M. C.; Warr, G. G. *J. Phys. Chem. B* **2010**, *114*, 1350–1360.
(19) Cabrerizo-Vilchez, M. A.; Wege, H. A; Holgado-Terriza, J. A.; Neumann, A. W. *Rev. Sci. Instrum.* **1999**, *70*, 2438–2444.
(20) Taboada, P.; Barbosa, S.; Castro, E; Mosquera, V. *J. Phys. Chem B* **2006**, *110*, 20733–20736.
(21) Jezequel, D.; Mayaffre, A.; Letellier, P. *J. Chim. Phys.* **1991**, *88*, 391–404.
(22) Gloton, M. P.; Mayaffre, A.; Turmine, M.; Letellier, P.; Suquet, H. *J. Colloid Interface Sci.* **1995**, *172*, 56–62.
(23) Poole, C. F. *J. Chromatogr., A* **2004**, *1037*, 49–82.
(24) Berr, S. S.; Caponetti, E.; Johnson, J. S., Jr.; Jones, R. R. M.; Magid, L. J. *J. Phys. Chem.* **1986**, *90*, 5766–5770.
(25) Berr, S. S. *J. Phys. Chem.* **1987**, *91*, 4760–4765.
(26) Šarac, B.; Bešter-Rogac, M. *J. Colloid Interface Sci.* **2009**, *338*, 216–221.
(27) Hoyer, H. W.; Marmo, A. *J. Phys. Chem.* **1961**, *65*, 1807–1810.
(28) González-Pérez, A.; Varela, L. M.; García, M.; Rodríguez, J. R. *J. Colloid Interface Sci.* **2006**, *293*, 213–221.
(29) Moulik, S. P.; Haque, E.; Jana, P.; Das, A. *J. Phys. Chem.* **1996**, *100*, 701–708.
(30) Jiang, N.; Li, P.; Wang, Y.; Wang, J.; Yan, H.; Thomas, R. K. *J. Colloid Interface Sci.* **2005**, *286*, 755–760.
(31) Nightingale, E. R., Jr. *J. Phys. Chem.* **1959**, *63*, 1381–1387.
(32) González-Pérez, A.; Czapkiewicz, J.; del Castillo, J. L.; Rodríguez, J. R. *Colloid Polym. Sci.* **2003**, *281*, 556–561.
(33) Mehta, S. K.; Bhasin, K. K.; Dham, S.; Singla, M. L. *J. Colloid Interface Sci.* **2008**, *321*, 442–451.
(34) Akba, H.; dem Batıgöç, Ç. *Colloid J.* **2008**, *70*, 127–133.
(35) Junquera, E.; Ortega, F.; Aicart, E. *Langmuir* **2003**, *19*, 4923–4932.
(36) Mata, J.; Varade, D.; Bahadur, P. *Thermochim. Acta* **2005**, *428*, 147–155.
(37) Abramoff, M. D.; Magelhaes, P. J.; Ram, S. J. *Biophotonics Int.* **2004**, *11*, 36–42.
(38) R Development Core Team *R: A Language and Environment for Statistical Computing*; R Foundation for Statistical Computing: Vienna, 2011.
(39) Kotlarchyk, M.; Stephens, J. R. B.; Huang, J. S. *J. Phys. Chem.* **1988**, *92*, 1533–1538.
(40) Provencher, S. W. *Comput. Phys. Commun.* **1982**, *27*, 213–227.
(41) Duvivier, S.; Turmine, M.; Letellier, P. *J. Chem. Soc., Faraday Trans.* **1998**, *94*, 3457–3461.